Carbohydrate Polymers 237 (2020) 116143

Contents lists available at ScienceDirect

Carbohydrate Polymers

journal homepage: www.elsevier.com/locate/carbpol

Structural characterization and anti-lung cancer activity of a sulfated glucurono-xylo-rhamnan from *Enteromorpha prolifera*

Weihua Jin[a,b,*], Xinyue He[a], Liufei Long[a], Qiufu Fang[a], Bin Wei[c], Jiadong Sun[d,e], Wenjing Zhang[f], Hong Wang[c], Fuming Zhang[b], Robert J. Linhardt[b,g]

[a] College of Biotechnology and Bioengineering, Zhejiang University of Technology, Hangzhou, 310014, China
[b] Department of Chemical and Biological Engineering, Center for Biotechnology and Interdisciplinary Studies, Rensselaer Polytechnic Institute, Troy, NY, 12180, USA
[c] Collaborative Innovation Center of Yangtze River Delta Region Green Pharmaceuticals & College of Pharmaceutical Sciences, Zhejiang University of Technology, Hangzhou, 310014, China
[d] Department of Biomedical and Pharmaceutical Sciences, College of Pharmacy, University of Rhode Island, Kingston, RI, 02881, USA
[e] Laboratory of Bioorganic Chemistry, National Institute of Diabetes and Digestive and Kidney Diseases (NIDDK), National Institutes of Health, Bethesda, MD, 20878, USA
[f] Department of Endocrinology, Sir Run Run Shaw Hospital, Zhejiang University School of Medicine, Hangzhou, 310016, China
[g] Department of Biological Science, Departments of Chemistry and Chemical Biology and Biomedical Engineering, Center for Biotechnology and Interdisciplinary Studies, Rensselaer Polytechnic Institute, Troy, NY, 12180, USA

ARTICLE INFO

Keywords:
Glucurono-xylo-rhamnan
Anti-lung cancer activity
Growth factor
Interaction
Surface plasmon resonance

ABSTRACT

A sulfated glucurono-xylo-rhamnan (EP-3-H) was purified from a green alga, *Enteromorpha prolifera*. EP-3-H and its oligomers were characterized by high performance liquid chromatography, mass spectrometry and one and two-dimensional nuclear magnetic resource spectroscopy. The structural analysis showed EP-3-H has a backbone of glucurono-xylo-rhamnan, branches with glucuronic acid and sulfated at C3 of rhamnose and/or C2 of xylose. The inhibition of EP-3-H on human lung cancer A549 cell proliferation *in vitro* and its therapeutic effects in BALB/c-nu mice *in vivo* were determined to evaluate the anti-lung cancer activity of EP-3-H. The tumor inhibition level was 59 %, suggesting that EP-3-H might be a good candidate for the treatment of lung cancer. Surface plasmon resonance (SPR) studies revealed the IC_{50} on the binding of fibroblast growth factors, (FGF1 and FGF2), to heparin were 0.85 and 1.47 mg/mL, respectively. These results suggest that EP-3-H inhibits cancer proliferation by interacting with these growth factors.

1. Introduction

Enteromorpha prolifera polysaccharides (EP) exhibit the superior moisture absorption and water retention properties (Shao et al., 2019) in addition it shows various bioactivities, including anticoagulant (Cui, Li, Wang et al., 2018, Cui, Li, Yu et al., 2018), immunomodulatory (Kim, Cho, Karnjanapratum, Shin, & You, 2011; Wei et al., 2014), hypolipidemic (Tang, Gao, Wang, Wen, & Qin, 2013; Teng, Qian, & Zhou, 2013) and anti-diabetic activities (Lin et al., 2015). Some researchers have also studied the mechanisms of the bioactivities of EP. For example, *in vivo* pre-treatment with EP in rats ameliorated acute myocardial infarction by reducing the infarct size and enhancing cardiac function and up-regulating HIF-1α. Moreover, EP activates the MEK/ERK and mTOR pathways while inactivating the NF-κB pathway in oxygen and glucose deprived human cardiac microvascular endothelial cells *in vitro* (Wang, Zhang, Zhao, Yong, & Mao, 2019). Oral administration of EP decreases serum triglyceride levels by increasing hydrogen sulfide production, suppresses sterol regulatory element binding protein-2 and lowers hepatic MG-CoA reductase mRNA protein expression in rats, suggesting that it is beneficial for the treatment of non-alcoholic fatty liver disease and reducing the risk of cardiovascular disease (Ren et al., 2017, 2018).

The controlled degradation and modification of EP have been performed in an effort to improve its pharmacological properties. Polysaccharides (44.1 kDa) obtained through enzymatic degradation from EP were able to ameliorate diabetes mellitus (Yuan et al., 2019). Low molecular weight EP and sulfated EP also showed improved moisture and absorption/retention abilities (Li, Chi, Yu, Jiang, & Liu, 2017, Li, Liu et al., 2017). Partially degraded EP also exhibits antibacterial activity (Lu, Gao, Shan, & Lin, 2014). Carboxymethylated, hydroxamidated partially degraded EP shows potent antioxidant ability (Ahn, Park, & Je, 2012; Li et al., 2013; Shao et al., 2017; Shi et al., 2017). In addition, the oral administration to rats of sulfated rhamnose polysaccharides with chromium (III) significantly improves oral glucose

* Corresponding author at: College of Biotechnology and Bioengineering, Zhejiang University of Technology, Hangzhou 310014, China.
E-mail address: jinweihua@zjut.edu.cn (W. Jin).

https://doi.org/10.1016/j.carbpol.2020.116143
Received 12 December 2019; Received in revised form 27 January 2020; Accepted 7 March 2020
Available online 09 March 2020
0144-8617/

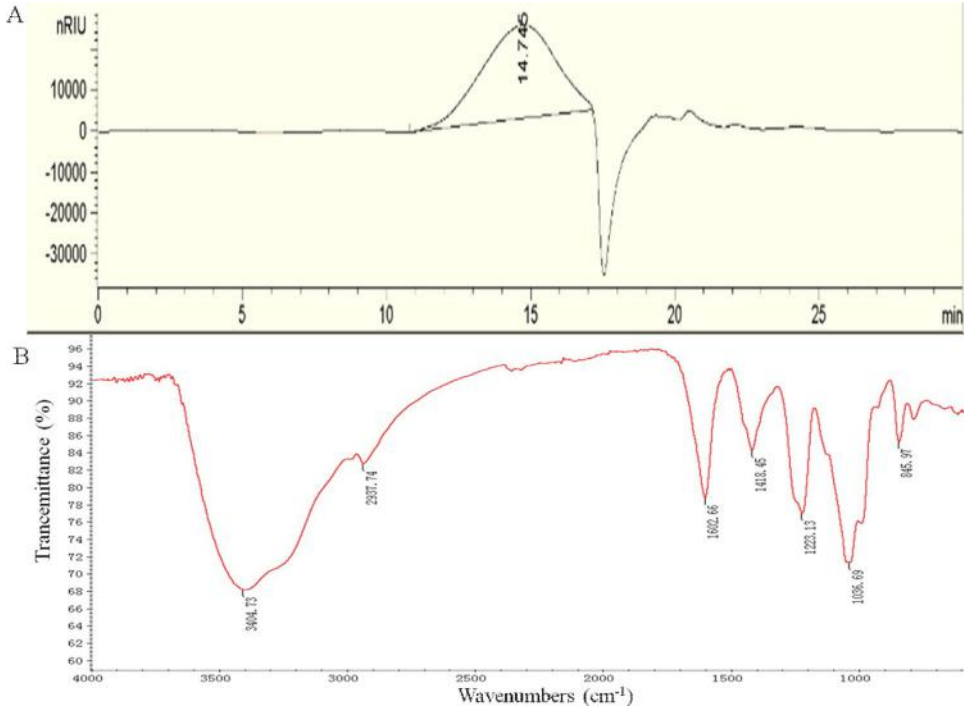

Fig. 1. GPC-HPLC chromatogram (A) and IR spectrum (B) of EP-3-H.

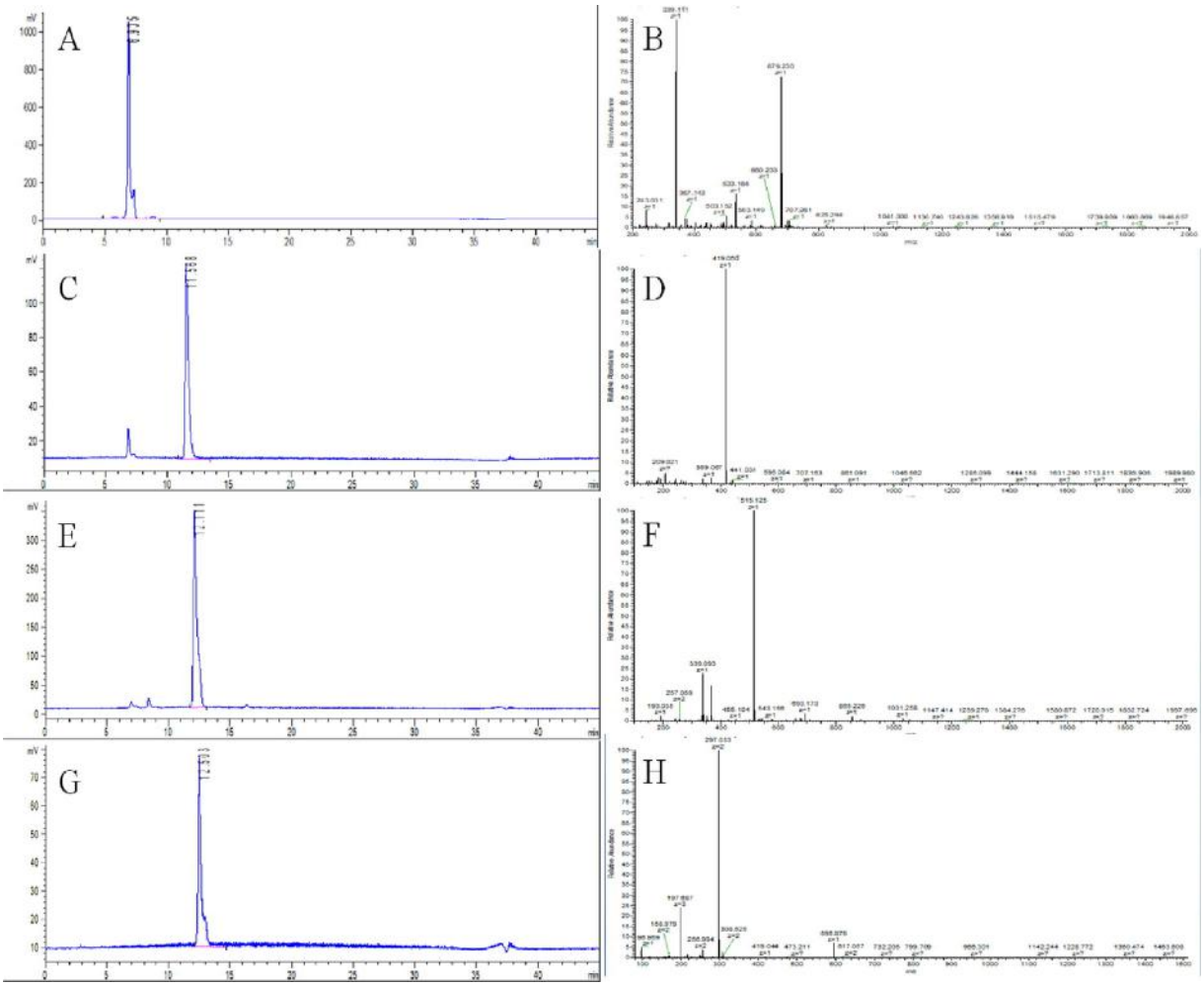

Fig. 2. HPLC chromatogram and negative-ion ESI mass spectra of oligomers from EP-3-H: GR (A and B), GRS (C and D), G2R (E and F) and G2RS (G and H).

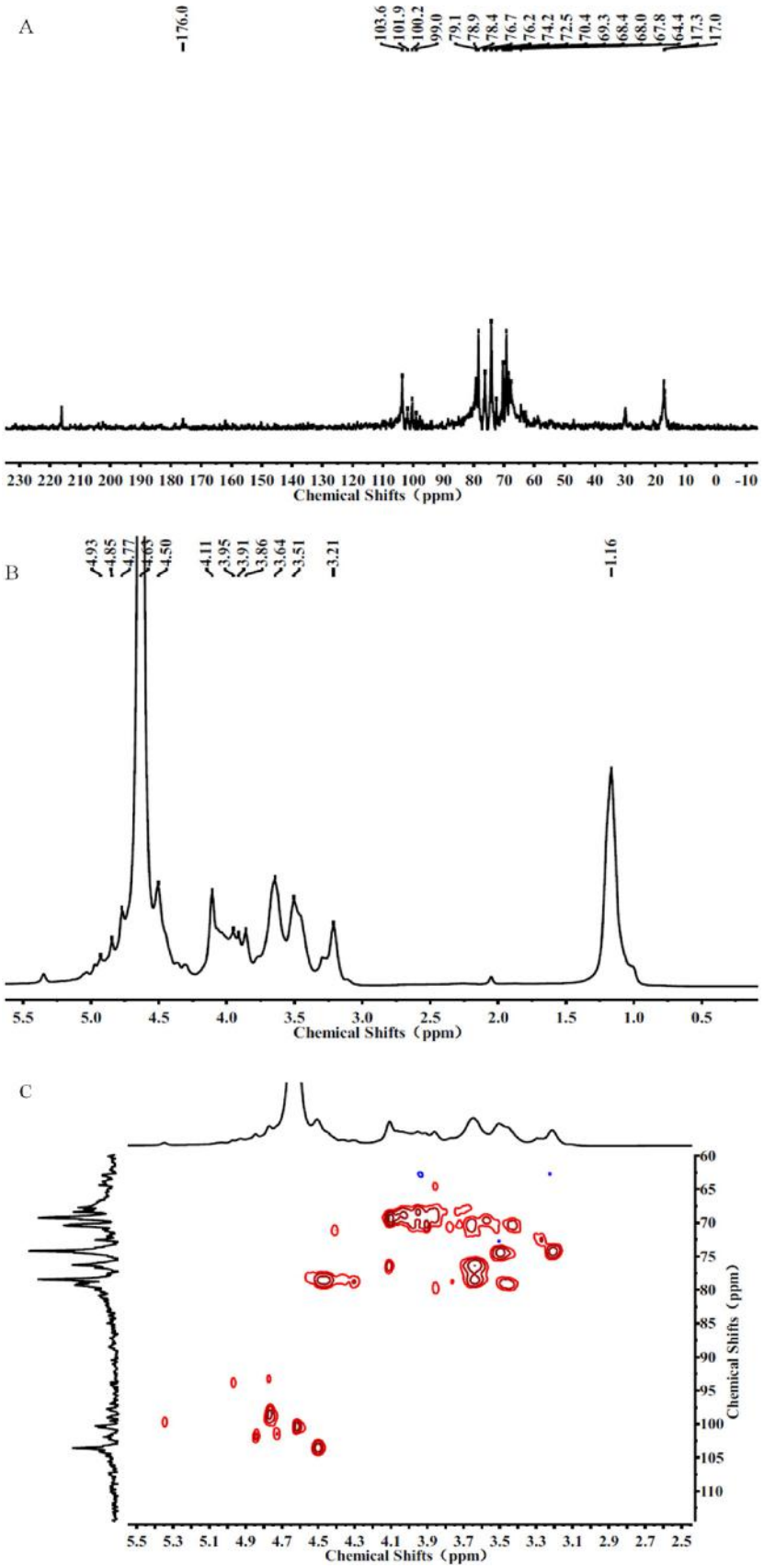

Fig. 3. The ^{13}C spectrum (A), ^{1}H-NMR spectrum (B) and HSQC spectrum (C) of EP-3-H.

tolerance, decreasing body mass gain, reduced serum insulin levels and increased tissue glycogen content, suggesting that it has therapeutic effect for the treatment of type-2 diabetic mellitus (Cui et al., 2019; Ye et al., 2019). EP-iron (III) complex displayed effects on rats with iron deficiency anemia (Chi et al., 2018; Cui, Li, Wang et al., 2018, Cui, Li, Yu et al., 2018). Moreover, EP-based nanoparticles have been used in controllable hydrophobic anti-tumor drug delivery (Li et al., 2018).

EP belongs to a family of sulfated heteropolysaccharides. Products of enzymatic hydrolysis have been purified by diethylaminoethyl (DEAE) cellulose-52 chromatography and Sephadex G-100 chromatography affording fractions, PHPE1, PHPE2, and PHPE3. PHPE-2 consisted of mannose, xylose and glucose (Xu et al., 2015). Enzymatic hydrolysis of EP showed that two different enzymes, DPE-L and DPE-P from *Alteromonas sp*. A321 afforded oligosaccharide products. Treatment with DPE-L resulted in $Rha(SO_3^-)$, $Rha(SO_3^-)GlcA$, $Rha_2(SO_3^-)_2GlcA$ and $Rha_3(SO_3^-)_3GlcAXyl$ while treatment with DPE-P produced Glc_2, Glc_3 and Glc_4 (Li et al., 2016). Another study demonstrated that EP had a backbone consisting of D-Glc*p*A-α-(1→4)-3-SO_3^- -L-Rha*p*-β-(1→4)-D-Xyl*p*-β-(1→4)-3-SO_3^--L-Rha*p* units (Yu, Li, Du, Mou, & Wang, 2017).

In this study, a sulfated glucurono-xylo-rhamnan (EP-3-H) was isolated from EP. Oligomers from acid degraded products of EP-3-H were separated and purified by anion exchange chromatography and gel filtration chromatography. The oligomers were subjected to structural analysis using high performance liquid chromatography (HPLC), mass spectrometry (MS) and one-dimensional (1D) nuclear magnetic resonance (NMR) spectroscopy. EP-3-H was further characterized by two-dimensional (2D) nuclear magnetic resonance (NMR) spectroscopy. The anticancer activity of EP-3-H was investigated by *in vitro* testing the proliferation inhibition on A549 cells and *in vivo* assessment of the tumor progression using BALB/c-nu mice. SPR was used to analyze the inhibition activity of EP-3-H on fibroblast growth factor (FGF1 and FGF2) binding to heparin. These results elucidated the structure of a sulfated glucurono-xylo-rhamnan (EP-3-H) and demonstrated its mechanism of anti-lung cancer activity.

2. Materials and methods

2.1. Preparation of EP-3-H and its derivates

Crude polysaccharide (EP) was extracted from *Enteromorpha prolifera* by hot water extraction using previously described methods (Jin, Zhang, Liang, & Zhang, 2016). Anion exchange chromatography on a DEAE-Bio Gel agarose FF Gel (6 cm × 40 cm) was performed with elution with water (EP-1), 0.3 M NaCl (EP-2), 1 M NaCl (EP-3) and 4 M NaCl (EP-4). The resulting polysaccharide fractions were dialyzed sing 500 Da cut-off membranes, concentrated, and precipitated using ethanol. Autohydrolysis of EP-3 was performed using a modification of a previously described method (Anastyuk, Imbs, Shevchenko, Dmitrenok, & Zvyagintseva, 2012). Briefly, EP-3 (0.8 g) was converted to the H^+-form using a cation exchange column. The H^+-form of EP-3 was kept at room temperature for 72 h for autohydrolysis, then neutralized with 5% NH_4OH solution. The product (named EP-3-H) from autohydrolysis was concentrated and precipitated by ethanol.

EP-3-H was degraded with 4% sulfuric acid, precipitated with ten-fold ethanol and fractionated using anion exchange chromatography by elution with water (EP-3-H-L1), 0.05 M NaCl (EP-3-H-L2), 0.1 M NaCl (EP-3-H-L3) and 2 M NaCl (EP-3-H-L4) based on a previously described method (Jin, Wang, Ren, Song, & Zhang, 2012). The resulting four fractions were further purified on a Bio-Gel P-4 Gel column (2.6 × 100 cm) to obtain EP-3-H-L1-1, EP-3-H-L1-2, EP-3-H-L1-3, EP-3-H-L2-1, EP-3-H-L2-2, EP-3-H-L3-1, EP-3-H-L3-2, EP-3-H-L4-1, EP-3-H-L4-2 and EP-3-H-L4-3, respectively.

2.2. Compositional analysis

The molar ratio of monosaccharides and fucose contents were determined as previously described (Zhang, Zhang, Wang, Shi, & Zhang, 2009). Briefly, polysaccharides (10 mg/mL) were hydrolyzed by trifluoroacetic acid (2 M) under a nitrogen atmosphere for 4 h at 110 °C. The hydrolyzed mixture was neutralized to pH 7 with sodium hydroxide, then was converted into its PMP derivatives and separated by high performance liquid chromatography (HPLC) on an YMC Pack ODS AQ column (4.6 × 250 mm, YMC, Kyoto, Japan). The sulfated contents were performed by a modification of a previously described method (Kawai, Seno, & Anno, 1969). Briefly, polysaccharides (25 mg/mL) were hydrolyzed by hydrochloric acid (2 M) under a nitrogen atmosphere for 4 h at 110 °C. The hydrolyzed mixture was neutralized to pH 7 with ammonium hydroxide, then was discolored by active carbon with barium chloride-gelatin reagent. Finally, the absorbance at 500 nm was detected by UV–vis Spectroscopy. The molecular weights of the polysaccharides were measured by gel permeation chromatography (GPC)-HPLC on TSK G3000 PWxl column (7 μm 7.8 × 300 mm) with elution in 0.05 M Na_2SO_4 at a flow rate of 0.5 mL/min at 40 °C using refractive index detection. Ten different molecular weight dextrans (2.5, 4.6, 7.1, 21.4, 41.1 and 133.8 k Da), purchased from the National Institute for the Control of Pharmaceutical and Biological Products (China), were used as molecular weight standards.

2.3. MS analysis of oligosaccharides

Electrospray ionization (ESI)-MS and ESI-chemically induced dissociation (CID)-MS/MS were performed on a LTQ ORBITRAR XL (Thermo Scientific). The samples were dissolved in CH_3CN-H_2O (1:1, v/v). Mass spectra were acquired in the negative-ion mode at a flow rate of 5 μL min^{-1}. The capillary voltage was set to −3000 V, and the cone voltage was set at −50 V. The source temperature was 80 °C, and the desolvation temperature was 150 °C. The collision energy was optimized between 10 and 50 eV. All spectra were analyzed using Xcalibur.

2.4. NMR spectroscopy

^{13}C-NMR, ^1H-NMR and 2D NMR (^1H-^1H correlated spectroscopy (COSY), ^1H-^{13}C heteronuclear single quantum coherence spectroscopy (HSQC), ^1H-^{13}C heteronuclear multiple bond correlation spectroscopy (HMBC) and ^1H-^1H total correlation spectroscopy TOCSY) spectra were recorded at a Bruker AVANCE III 600 MHz (Bruker BioSpin, Billerica, MA, USA) at 25 °C. The chemical shifts were adjusted to the internal standard (deuterated acetone, 2.05 and 29.92 ppm, respectively).

2.5. The proliferation inhibition activity

The proliferation inhibition activities of polysaccharides against human lung cancer A549 cells were determined. A 3-(4, 5-dimethylthiazol-2-yl)-2, 5-diphenyl tetrazolium (MTT) assay was used to measure cell viability. The cells were divided into two groups: (1) a control group in which cells were cultivated in blank medium and (2) an experimental group in which cells and EP-3-H at different concentrations were cultivated in medium. Inhibition was determined using the following equation: Cell Inhibition (%) = (Ac − A1)/(Ac − A0) × 100, where A0 was the absorbance of the blank medium (no cells), A1 was the absorbance in the presence of samples, and Ac was the absorbance of the control.

2.6. Xenograft tumor model

Four-week-old male BALB/c-nu nude mice were purchased from Shanghai Sipu-Bikai Experimental Animal Co., LTD (Shanghai, China). The protocol for all studies with mice was approved (approval # ZJUT-20180101) by the Zhejiang University of Technology Animal Center in

Table 1
^{1}H and DEPTQ chemical shifts of NMR spectra of EP-3-H.

	Residues	H1/C1	H2/C2	H3/C3	H4/C4	H5/C5	H6/C6
A	→4)-α-L-Rha*p*(3-SO_3^-)-(1→	4.85 /101.9	3.86-4.11 /67.8-69.3	4.50 /78.4-79.1	3.64 /76.7	3.91 /70.4	1.16 /17.3,17.0
B	→4)-α-L-Rha*p*-(1→	4.77 /99.0	3.95 /70.4	4.11 /70.4	3.91 /78.4-79.1	3.86 /70.4	1.16 /17.3,17.0
C	→4)-α-L-Rha*p*(3-SO_3^-)-(1→	4.77 /101.9	3.86-4.11 /67.8-69.3	4.50 /78.4-79.1	3.64 /76.7	3.91 /70.4	1.16 /17.3,17.0
D	→4)-β-D-Glc*p*A-(1→	4.63 /100.2	3.21 /74.2	3.51 /74.2	3.64 /78.4-79.1	3.64 /76.2	– /176.0
E	β-D-Glc*p*A-(1→2	4.50 /103.6	3.21 /74.2	3.51 /74.2	3.27 /72.5	3.64 /76.2	– /176.0
F	→4)-β-D-Xyl*p*-(1→	4.50 /103.6	3.21 /74.2	3.51 /74.2	3.64 /76.7	3.86 /64.4	– /-
G	→2,4)-α-L-Rha*p*(3-SO_3^-)-(1→	4.93/ 103.6	3.86-4.11 /67.8-69.3	4.50 /78.4-79.1	3.64 /76.7	3.91 /70.4	1.16 /17.3,17.0

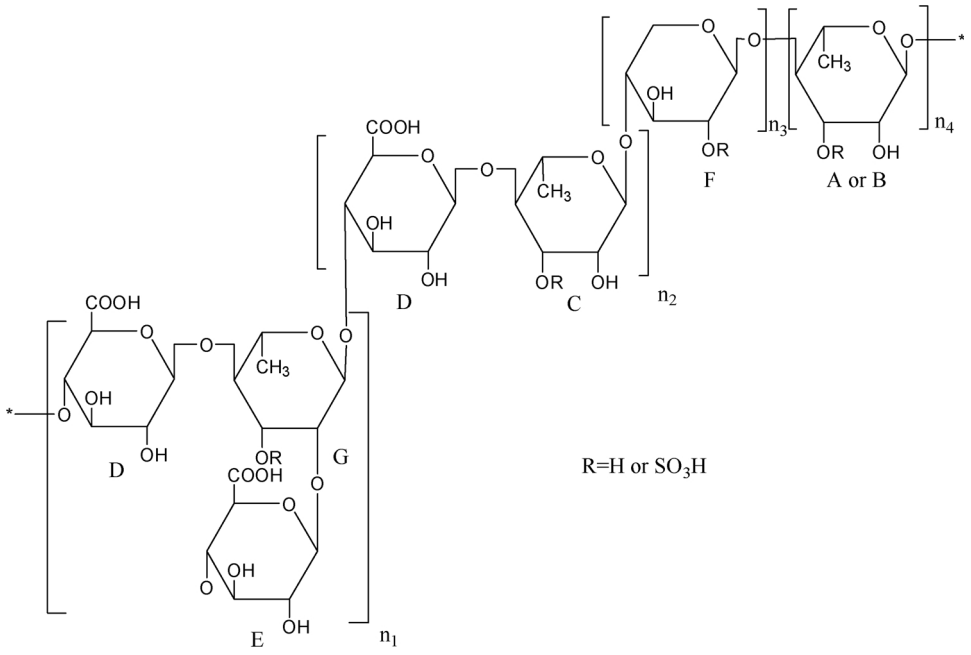

Scheme 1. Proposed structure of EP-3-H.

accordance with the animal care and use guidelines. Tumors were established by giving a *subcutaneous* injection of 2.5×10^6 (0.2 mL) A549 cells into the right flank of the mouse. Xenograft mice were administrated EP-3-H as an *i.p.* dose at 100 mg/kg (0.2 mL) every day, while an equal volume of normal saline was injected as a control. Drug-treatment was initiated after tumors were palpable and lasted for 21 days. Body weight and tumor volumes were measured every two days with a balance and with a vernier caliper, respectively. The tumor volume was calculated with the formula: $V = ½ \times \text{length} \times \text{width}^2$ and the relative tumor volume (RTV) was calculated with the formula: V_n/V_0 (V_n corresponds to the tumor volume at the "n" day after administration and V_0 represents the tumor volume before administration). After three weeks of treatment, the mice were euthanized to excise tumors. Tumor inhibition was calculated according to the following formula: (the mean tumor weight of control group - the mean tumor weight of treated group)/the mean tumor weight of control group × 100. The organ coefficients of nude mice were calculated as follows: organ weight × 1000/body weight.

2.7. Solution competition study between heparin on chip surface and EP-3-H in solution using surface plasmon resonance (SPR)

Solution competition SPR measurements were performed on a BIAcore 3000 (GE Healthcare, Uppsala, Sweden). Heparin chip was prepared according to the previous studies (Zhang et al., 2019) by the immobilization of biotinylated heparin on a streptavidin (SA) chip. To prepare biotinylated heparin, heparin (2 mg) and amine–PEG3–Biotin (2 mg, Thermo Scientific, Waltham, MA, USA) were mixed with $NaCNBH_3$ (10 mg) in 0.2 mL water. The initial reaction was carried out at 70 °C for 24 h, and then a further $NaCNBH_3$ (10 mg) was added for another 24 h. Later, the mixture was desalted with a spin column (3000 molecular weight cut-off) and freeze-dried. The biotinylated heparin was immobilized to a SA chip based on the manufacturer's protocol. In brief, a 20 μL solution of the heparin-biotin conjugate (0.1 mg/mL) in HBS-EP buffer (0.01 M HEPES, 0.15 M NaCl, 3 mM EDTA, 0.005 % surfactant P20, pH 7.4) was injected over flow cell 2 (FC2), 3 (FC3) and 4 (FC4) of the SA chip at a flow rate of 10 μL/min. The successful immobilization of heparin was confirmed by the observation of a ~100 resonance unit (RU) increase in the sensor chip. The control flow cell (FC1) was prepared by 1 min injection with saturated biotin. To measure the inhibition of EP-3-H on fibroblast growth factors (FGF1 and

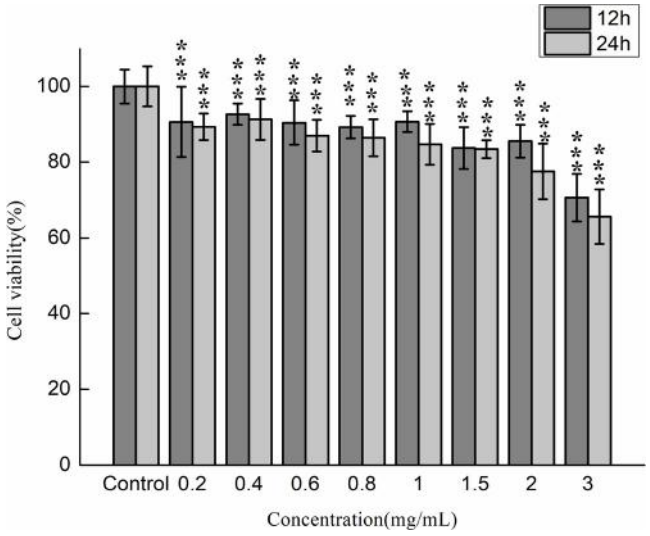

Fig. 4. Concentration-dependent and time-dependent cytotoxic effects of EP-3-H on A549 cells. Cells were cultured in 96-well plate and treated with different doses of EP-3-H (0.2-3.0 mg/mL) for 12 and 24 h. The cell viability was analyzed by MTT assay. Data are presented as mean ± SD of more than three independent experiments (n > 3). *** $p < 0.001$, ** $p < 0.01$ *versus* Control.

FGF2) binding to heparin surface, FGF1 or FGF2 was pre-mixed with different concentrations of EP-3-H (0, 1/16, 1/8, 1/4, 1/2, 1 and 2 mg/mL) and injected over the heparin chip at 30 μL/min. After each run, a dissociation period and regeneration with 2 M NaCl was performed.

2.8. Statistical analysis

All data are shown as the mean ± standard deviation (SD). Significant differences between experimental groups were determined by one-way ANOVA, and differences were considered as statistically significant if $p < 0.05$. All calculations were performed using SPSS 16.0 Statistical Software.

3. Results and discussion

3.1. Chemical compositions analysis of EP-3-H

The extraction yield of EP-3-H from EP-3 was 62 %. The chemical compositional analysis of EP-3-H showed the contents of rhamnose, sulfate and total sugar in EP-3-H were 46 %, 16 % and 80 %, respectively, and the molar ratio of the EP-3-H monosaccharides, rhamnose (Rha), glucuronic acid (GlcA) and xylose (Xyl) were Rha:GlcA:Xyl = 1:0.41:0.12, suggesting that EP-3-H is a glucurono-xylo-rhamnan. GPC-HPLC analysis showed the average molecular weight of EP-3-H is 7.7 kDa (Fig. 1A). The IR spectrum (Fig. 1B) shows bands at 1223 cm^{-1} attributed to the asymmetric O═S═O stretching vibration of sulfate half esters and bands at approximately 846 cm^{-1} attributed to the C—O—S bending vibration of the sulfate substituents at the axial C2 or C3 positions of rhamnose, suggesting that sulfation pattern was at the C2 or C3 positions of rhamnose (Foley, Mulloy, & Tuohy, 2011; Synytsya et al., 2010).

3.2. Structure analysis of EP-3-H

EP-3-H was degraded with 4% sulfuric acid, precipitated with ten-fold ethanol and fractionated by anion exchange chromatography eluted with water (EP-3-H-L1), 0.05 M NaCl (EP-3-H-L2), 0.1 M NaCl (EP-3-H-L3) and 2 M NaCl (EP-3-H-L4). The negative-ion ESI mass spectra of the fractions are shown in the Supplementary data (Fig S1-S4). All fractions were purified by gel filtration chromatography to obtain oligomers. The HPLC chromatograms of all fractions are presented in Supplementary data (Fig S5-S8). NMR spectroscopy was performed to analyze four major oligosaccharides, dimer GR, trimer G_2R, sulfated dimer GRS and sulfated trimer G_2RS (Fig S9-S12). The structures were established as GR, β-D-Glc*p*A(1→4)-α/β-L-Rha*p*; GRS, β-D-Glc*p*A(1→4)-α/β-L-Rha*p* (3-SO_3^-); G_2R, β-D-Glc*p*A(1→4)-[β-D-Glc*p*A(1→2)-]-α/β-L-Rha*p*; and G_2RS, β-D-Glc*p*A(1→4)-[β-D-Glc*p*A(1→2)-]-α/β-L-Rha*p* (3-SO_3^-) (Lahaye & Ray, 1996). The HPLC chromatograms and MS spectra of these oligosaccharides are shown in Fig. 2.

^{13}C-NMR, ^{1}H-NMR and 2D NMR spectroscopy of EP-3-H were performed to elucidate their structure. The ^{13}C-NMR, ^{1}H-NMR and 2D NMR spectra were shown in Fig. 3 and Fig S13. There were four major signals in the heteronuclear single quantum coherence (HSQC) spectrum. The anomeric proton signal at 4.85 ppm correlated to the anomeric carbon signal at 101.9 ppm, which was attributed to 4-linked 3-sulfated α-L-Rha*p* residues. The proton signal at 4.77 ppm correlated to two anomeric carbon signals at 99.0 ppm (major) and 101.9 ppm (minor, signal was not shown), which were attributed to the 4-linked α-L-Rha*p* residues and 4-linked 3-sulfated α-L-Rha*p* residues. The proton signal at 4.63 ppm correlated to the anomeric carbon signal at 100.2 ppm, which was attributed to 4-linked β-D-Glc*p*A residues. The weak proton signal at 4.93 ppm correlated to the anomeric carbon signal at 103.6 ppm, which was attributed to the 2, 4-linked 3-sulfated α-L-Rha*p* residues. The proton signal at 4.50 correlated to the anomeric carbon signal at 103.6 ppm, which was attributed to the non-reducing end β-D-Glc*p*A residues and 4-linked β-D-Xyl*p* residues. The heteronuclear multiple bond correlation (HMBC) spectrum (Fig S13) confirmed some of the linkages and the sequence of the sugar residues. The anomeric proton signal at 4.85 ppm correlated to the C-4 signal at 78.4–79.1 ppm, suggesting a 1→4 linkage of residue A to residues B/D. The anomeric proton signal at 4.50 ppm also correlated to the C-4 signal at 78.4–79.1 ppm, suggesting that a 1→4 linkage of residue F to residue B. The ^{1}H and distortionless enhancement by polarization transfer including quaternary nuclei (DEPTQ) chemical shifts of EP-3-H are summarized in Table 1.

Based on previous studies (Kidgell, Magnusson, de Nys, & Glasson, 2019; Lahaye & Ray, 1996; Lahaye, Brunel, & Bonnin, 1997; Lahaye, 1998; Li, Chi et al., 2017; Li, Liu et al., 2017, Li, Guo, Wang, Wang, & Li, 2019, Li, Wang et al., 2019; Wang et al., 2020) and by combining with the structures of the oligosaccharides determined in this study we propose that EP-3-H has a backbone of glucurono-xylo-rhamnan, branches with Glc*p*A and sulfated at C3 of Rha*p* and/or C2 of Xyl*p*. Scheme 1 shows the proposed structure of EP-3-H.

3.3. EP-3-H inhibition on the proliferation of A549 cells

A549 cells were exposed to increasing concentrations of EP-3-H for 12 and 24 h to evaluate the proliferation inhibition by EP-3-H. EP-3-H slightly inhibited the growth of A549 cells (Fig. 4). The inhibition at a dose of 3.0 mg/mL SGRA for 12 and 24 h was 29 % and 34 %, respectively. The percentage inhibitions in Fig S14 of GR, GRS, G_2R and G_2RS at the concentration of 1.82 mg/mL for 24 h were 49 %, 54 %, 5% and 34 %, respectively. The IC_{50} of polysaccharides from *Inonotus obliquus* on Lewis lung carcinoma LLC1 cells was reportedly 0.39 mg/mL at 24 h (Jiang et al., 2019). Two polysaccharides from *Psoralea corylifolia L* exhibited significant anti-A549 lung cancer cells activity with IC_{50} values of 64.8 and 126.3 μM (Yin et al., 2019). CMPS-II and CBPS-II polysaccharides from the fermented mycelium and cultivated fruiting bodies of *Cordyceps militaris* exhibited 55 and 35 % inhibition at a concentration of 0.5 mg/mL after 44 h on human non-small cell lung cancer H1299 cells (Liu, Zhu, Liu, & Sun, 2019). Compared to these previously studied polysaccharides, EP-3-H showed lower cytotoxicity, suggesting that EP-3-H could be a good candidate for the treatment of lung cancer.

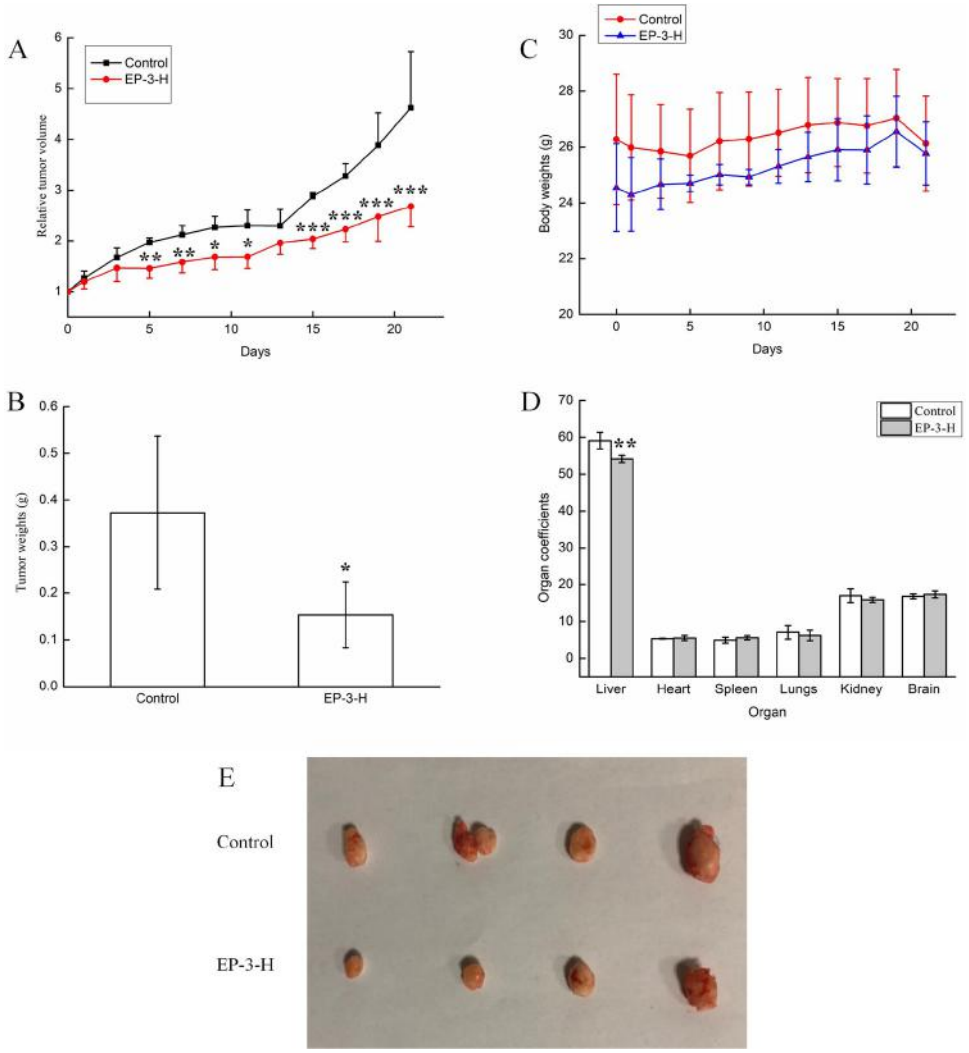

Fig. 5. Attenuation of A549 cell xenograft tumor growth in BALB/c-nude mice by EP-3-H. (**A**) The relative tumor volume (RTV) of each group. *** $p < 0.001$, ** $p < 0.01$, * $p < 0.05$ *versus* control (**B**) Tumor weight of each group. * $p < 0.05$ *versus* control. (**C**) The effects on the body weights of treated mice. (**D**) The organ coefficients of nude mice. * $p < 0.05$ *versus* control. (**E**) Representative images of the A549 xenograft tumors from each group at day 21.

3.4. Anti-lung cancer activity of EP-3-H

We next evaluated the therapeutic effects of EP-3-H in BALB/c-nu mice to determine whether EP-3-H could suppress the growth of tumor *in vivo* (Fig. 5). After 21 days treatment, the relative tumor volumes (RTV) data (Fig. 5A) showed EP-3-H significantly attenuated A549 xenograft tumors compared with the control group. The tumor inhibition (Fig. 5B) was 59 % while GRS did not exhibit any inhibition in Fig S15. Mouse body weights (Fig. 5C) in EP-3-H groups fluctuated, increasing slightly, while mice in the control group maintained a stable weight except on the final day. The organ coefficients of nude mice are shown in Fig. 5D. The organ coefficients of liver in EP-3-H group decreased slightly compared with the control group. It has been reported that the oral administration of Fucoidan-Sargassum polysaccharide (1 g/kg) over five weeks showed about 63 % inhibition (Pan et al., 2019). Oral administration of polysaccharides from *Sargassum fusiforme* (200 mg/kg) for four weeks showed about 43 % inhibition (Fan et al., 2018). Peritoneal injection with 20 mg/kg/d cyclophosphamide and 600 mg/kg Yulangsan polysaccharide administered for 2 weeks exhibited 45 and 40 % inhibition, respectively (Qin et al., 2019). Compared to these treatments, the anti-lung cancer activity of EP-3-H was similar to the drug cyclophosphamide and better than the other polysaccharides. In addition, EP-3-H is a purified polysaccharide, not a crude polysaccharide. Therefore, we suggest that EP-3-H represents an excellent therapeutic candidate for the treatment of lung cancer.

3.5. SPR solution competition study between EP-3-H and growth factors

Very strong inhibitory activity (> 80 %) towards FGF1 was observed on EP-3-H concentration of 2.0 mg/mL (Fig. 6A and B). The half maximal inhibitory concentration (IC_{50}) was 0.85 mg/mL. In Fig. 6C and D, strong inhibitory activity (> 60 %) was observed for FGF2 at a concentration of 2.00 mg/ml and its IC_{50} was 1.47 mg/mL. Tumor angiogenesis is a complex, multistep cascade involving the activation of endothelial cells by heparan sulfate-binding, angiogenic growth factors (such as VEGF, FGF1 and FGF2), resulting in endothelial cell proliferation and migration and ultimately, new blood vessel formation (Cochran et al., 2003). In addition, FGFs also participate in regulating cell growth, survival differentiation and migration, which is mediated by binding to and activating cell surface tyrosine kinase FGF receptors (FGFRs) (Peelen et al., 2006). FGF1 and FGF2, members of FGF family, contribute to the formation of a ternary complex between FGF, FGFR and heparin/heparan sulfate. Complex formation is the key step for the activation of the FGF signaling pathway, which is at the origin of different cellular essential functions (Munoz-Garcia et al., 2014). FGF1 and FGF2 display important roles in angiogenesis, the regulation of

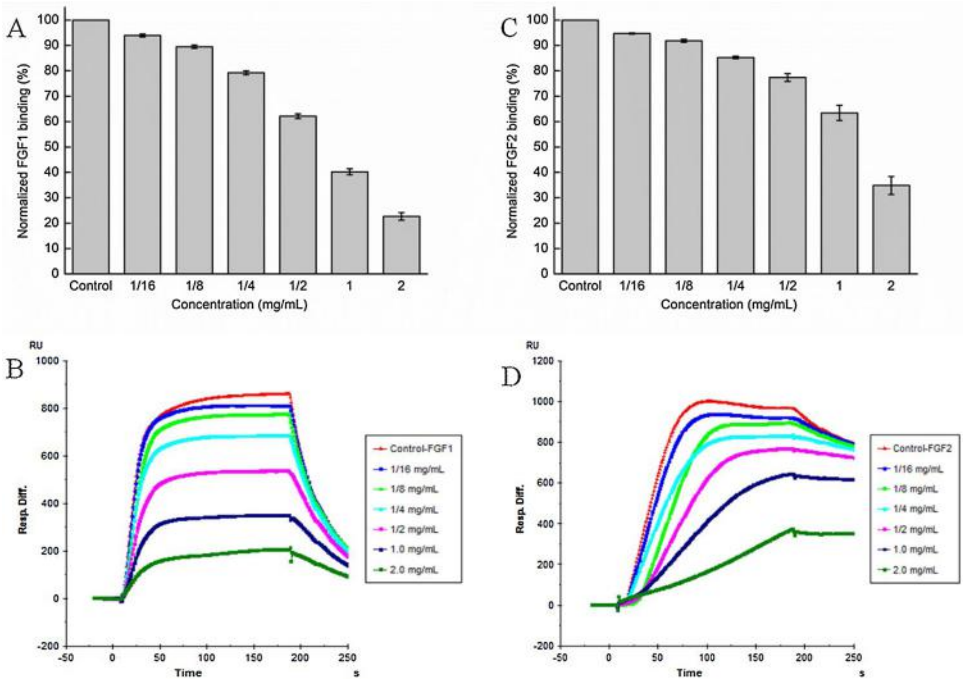

Fig. 6. Bar graphs and SPR sensorgrams of normalized different growth factors (FGF1 (A and B) and FGF2 (C and D)) binding preference to surface heparin by competing with different concentrations of EP-3-H. Concentrations were 125 nM and 100 nM for FGF1 and FGF2. Data are presented as mean ± SD of three independent experiments (n = 3).

extracellular matrix, cell differentiation, inflammatory responses, cell migration and invasion, which contributing to the development, progression and pathogenesis of tumor (Li, Guo et al., 2019, Li, Wang et al., 2019). The anti-cancer activity of EP-3-H might due to the inhibition of cancer cell proliferation through its interaction with growth factors.

4. Conclusion

EP-3-H was obtained from *Enteromorpha prolifera* using anion exchange chromatography after autohydrolysis. GPC showed a single peak at 14.7 min, suggesting EP-3-H was a single polysaccharide. Monosaccharide analysis showed that EP-3-H contained rhamnose, glucuronic acid and xylose in a molar ratio of 1:0.41:0.12. IR spectroscopy confirmed that rhamnose residues were sulfated at the C2 or C3 position. Thus, we confirmed that EP-3-H was a sulfated glucurono-xylo-rhamnan. Acid degradation was performed to elucidate the structure of EP-3-H. Four major oligosaccharides, GR, GRS, G_2R and G_2RS were obtained and characterized by HPLC, MS and NMR spectroscopy. GR was β-D-Glc*p*A(1→4)-α/β-L-Rha*p*, GRS was β-D-Glc*p*A(1→4)-α/β-L-Rha*p*(3-SO_3^-), G_2R was β-D-Glc*p*A(1→4)-[β-D-Glc*p*A(1→2)-]-α/β-L-Rha*p* and G_2RS was β-D-Glc*p*A(1→4)-[β-D-Glc*p*A(1→2)-]-α/β-L-Rha*p*(3-SO_3^-). These oligosaccharides correspond to the backbone units of EP-3-H. Further structural analysis, performed using one and 2D NMR spectroscopy, confirm that EP-3-H had a backbone of glucurono-xylo-rhamnan, with GlcAp and C3 sulfated Rha*p* and/or C2 sulfated Xyl*p*.

EP-3-H only slightly inhibited cell proliferation suggesting that it might be a non-toxic polysaccharide. An A549 cell xenograft tumor growth model in BALB/c-nude mice showed that EP-3-H showed 59 % inhibition, suggesting that EP-3-H might be a good candidate for the treatment of lung cancer. EP-3-H did not directly kill the cancer cells because of its low cytotoxicity, suggesting another mechanism for the inhibition of cancer cell proliferation. Growth factors could influence normal cell differentiation, and constitutive activation of growth-promoting pathways in cancer cells can modulate the cell phenotypes (Aaronson, 1991). FGF signalling activity is regulated by the binding specificity of ligands and receptors (Zhang et al., 2006). Therefore, we tested the binding affinity of growth factors interacting with EP-3-H by competition on heparin chip using SPR. The IC_{50} of normalized different growth factors FGF1 and FGF2 were 0.85 and 1.47 mg/mL, respectively, suggesting that EP-3-H might inhibit cancer cell proliferation by interacting with these growth factors. We believe our current study provides important insight into the application of polysaccharides in the development of anti-cancer therapeutics.

CRediT authorship contribution statement

Weihua Jin: Conceptualization, Methodology, Data curation, Formal analysis, Funding acquisition, Resources, Writing - original draft, Supervision, Project administration. **Xinyue He:** Conceptualization, Methodology, Investigation, Formal analysis. **Liufei Long:** Conceptualization, Methodology, Visualization. **Qiufu Fang:** Conceptualization, Methodology, Validation. **Bin Wei:** Methodology, Writing - review & editing. **Jiadong Sun:** Methodology, Writing - review & editing. **Wenjing Zhang:** Methodology, Writing - original draft, Writing - review & editing. **Hong Wang:** Writing - review & editing, Funding acquisition. **Fuming Zhang:** Methodology, Writing - review & editing. **Robert J. Linhardt:** Writing - review & editing.

Declaration of Competing Interest

The authors declare no conflicts of interest.

Acknowledgements

This study was supported by the National Key Research and Development Program of China (No. 2017YFE0103100); the Open Fund of Key Laboratory of Experimental Marine Biology, Chinese Academy of Sciences (No. KF2018NO2); the Zhejiang Provincial Natural Science Foundation of China (No. LY19D060006) and China Scholarship Council (W.J.).

Appendix A. Supplementary data

Supplementary material related to this article can be found, in the online version, at doi:https://doi.org/10.1016/j.carbpol.2020.116143.

References

Aaronson, S. A. (1991). Growth factors and cancer. *Science, 254*(5035), 1146–1153.

Ahn, C. B., Park, P. J., & Je, J. Y. (2012). Preparation and biological evaluation of enzyme-assisted extracts from edible seaweed (*Enteromorpha prolifera*) as antioxidant, anti-acetylcholinesterase and inhibition of lipopolysaccharide-induced nitric oxide production in murine macrophages. *International Journal of Food Sciences and Nutrition, 63*(2), 187–193.

Anastyuk, S. D., Imbs, T. I., Shevchenko, N. M., Dmitrenok, P. S., & Zvyagintseva, T. N. (2012). ESIMS analysis of fucoidan preparations from *Costaria costata*, extracted from alga at different life-stages. *Carbohydrate Polymers, 90*(2), 993–1002.

Chi, Y., Li, Y., Zhang, G., Gao, Y., Ye, H., Gao, J., et al. (2018). Effect of extraction techniques on properties of polysaccharides from *Enteromorpha prolifera* and their applicability in iron chelation. *Carbohydrate Polymers, 181*, 616–623.

Cochran, S., Li, C., Fairweather, J. K., Kett, W. C., Coombe, D. R., & Ferro, V. (2003). Probing the interactions of phosphosulfomannans with angiogenic growth factors by surface plasmon resonance. *Journal of Medicinal Chemistry, 46*(21), 4601–4608.

Cui, J. F., Ye, H., Zhu, Y. J., Li, Y. P., Wang, J. F., & Wang, P. (2019). Characterization and hypoglycemic activity of a rhamnan-type sulfated polysaccharide derivative. *Marine Drugs, 17*(1).

Cui, J., Li, Y., Wang, S., Chi, Y., Hwang, H., & Wang, P. (2018). Directional preparation of anticoagulant-active sulfated polysaccharides from *Enteromorpha prolifera* using artificial neural networks. *Scientific Reports, 8*(1), 3062.

Cui, J., Li, Y., Yu, P., Zhan, Q., Wang, J., Chi, Y., et al. (2018). A novel low molecular weight Enteromorpha polysaccharide-iron (III) complex and its effect on rats with iron deficiency anemia (IDA). *International Journal of Biological Macromolecules, 108*, 412–418.

Fan, S., Yu, G., Nie, W., Jin, J., Chen, L., & Chen, X. (2018). Antitumor activity and underlying mechanism of *Sargassum fusiforme* polysaccharides in CNE-bearing mice. *International Journal of Biological Macromolecules, 112*, 516–522.

Foley, S. A., Mulloy, B., & Tuohy, M. G. (2011). An unfractionated fucoidan from *Ascophyllum nodosum*: Extraction, characterization, and apoptotic effects in vitro. *Journal of Nature Products*110829092019063.

Jiang, S., Shi, F., Lin, H., Ying, Y., Luo, L., Huang, D., et al. (2019). *Inonotus obliquus* polysaccharides induces apoptosis of lung cancer cells and alters energy metabolism via the LKB1/AMPK axis. *International Journal of Biological Macromolecules* in press.

Jin, W. H., Wang, J., Ren, S. M., Song, N., & Zhang, Q. B. (2012). Structural analysis of a heteropolysaccharide from *Saccharina japonica* by electrospray mass spectrometry in tandem with collision-induced dissociation tandem mass spectrometry (ESI-CID-MS/MS). *Marine Drugs, 10*(10), 2138–2152.

Jin, W. H., Zhang, W. J., Liang, H. Z., & Zhang, Q. B. (2016). The structure-activity relationship between marine algae polysaccharides and anti-complement activity. *Marine Drugs, 14*(1).

Kawai, Y., Seno, N., & Anno, K. (1969). A modified method for chondrosulfatase assay. *Analytical Biochemistry, 32*(2), 314–321.

Kidgell, J. T., Magnusson, M., de Nys, R., & Glasson, C. R. K. (2019). Ulvan: A systematic review of extraction, composition and function. *Algal Research, 39*, 101422.

Kim, J. K., Cho, M. L., Karnjanapratum, S., Shin, I. S., & You, S. G. (2011). In vitro and in vivo immunomodulatory activity of sulfated polysaccharides from *Enteromorpha prolifera*. *International Journal of Biological Macromolecules, 49*(5), 1051–1058.

Lahaye, M. (1998). NMR spectroscopic characterisation of oligosaccharides from two *Ulva rigida* ulvan samples (Ulvales, Chlorophyta) degraded by a lyase. *Carbohydrate Research, 314*(1-2), 1–12.

Lahaye, M., & Ray, B. (1996). Cell-wall polysaccharides from the marine green alga Ulva "rigida" (Ulvales, Chlorophyta)–NMR analysis of ulvan oligosaccharides. *Carbohydrate Research, 283*, 161–173.

Lahaye, M., Brunel, M., & Bonnin, E. (1997). Fine chemical structure analysis of oligosaccharides produced by an ulvan-lyase degradation of the water-soluble cell-wall polysaccharides from Ulva sp, (Ulvales, Chlorophyta). *Carbohydrare Research, 304*(3-4), 325–333.

Li, B., Liu, S., Xing, R., Li, K., Li, R., Qin, Y., et al. (2013). Degradation of sulfated polysaccharides from *Enteromorpha prolifera* and their antioxidant activities. *Carbohydrate Polymers, 92*(2), 1991–1996.

Li, J., Jiang, F., Chi, Z., Han, D., Yu, L., & Liu, C. (2018). Development of Enteromorpha prolifera polysaccharide-based nanoparticles for delivery of curcumin to cancer cells. *International Journal of Biological Macromolecules, 112*, 413–421.

Li, Y., Li, W., Zhang, G., Lu, X., Hwang, H., Aker, W. G., et al. (2016). Purification and characterization of polysaccharides degradases produced by *Alteromonas sp*. A321. *International Journal of Biological Macromolecules, 86*, 96–104.

Li, J., Chi, Z., Yu, L., Jiang, F., & Liu, C. (2017). Sulfated modification, characterization, and antioxidant and moisture absorption/retention activities of a soluble neutral polysaccharide from *Enteromorpha prolifera*. *International Journal of Biological Macromolecules, 105*(Pt 2), 1544–1553.

Li, Y., Guo, X. B., Wang, J. S., Wang, H. C., & Li, L. P. (2019). Function of fibroblast growth factor 2 in gastric cancer occurrence and prognosis. *Molecular Medicine Reports* in press.

Li, N., Liu, X., He, X., Wang, S., Cao, S., Xia, Z., et al. (2017). Structure and anticoagulant property of a sulfated polysaccharide isolated from the green seaweed *Monostroma angicava*. *Carbohydrate Polymers, 159*, 195–206.

Li, Y., Wang, X., Jiang, Y., Wang, J., Hwang, H., Yang, X., et al. (2019). Structure characterization of low molecular weight sulfate Ulva polysaccharide and the effect of its derivative on iron deficiency anemia. *International Journal of Biological Macromolecules, 126*, 747–754.

Lin, W., Wang, W., Liao, D., Chen, D., Zhu, P., Cai, G., et al. (2015). Polysaccharides from *Enteromorpha prolifera* improve glucose metabolism in diabetic rats. *Journal of Diabetes Research, 2015*, 675201.

Liu, X. C., Zhu, Z. Y., Liu, Y. L., & Sun, H. Q. (2019). Comparisons of the anti-tumor activity of polysaccharides from fermented mycelia and cultivated fruiting bodies of *Cordyceps militaris in vitro*. *International Journal of Biological Macromolecules, 130*, 307–314.

Lu, H., Gao, Y., Shan, H., & Lin, Y. (2014). Preparation and antibacterial activity studies of degraded polysaccharide selenide from *Enteromorpha prolifera*. *Carbohydrate Polymers, 107*, 98–102.

Munoz-Garcia, J. C., Garcia-Jimenez, M. J., Carrero, P., Canales, A., Jimenez-Barbero, J., Martin-Lomas, M., et al. (2014). Importance of the polarity of the glycosaminoglycan chain on the interaction with FGF-1. *Glycobiology, 24*(11), 1004–1009.

Pan, T. J., Li, L. X., Zhang, J. W., Yang, Z. S., Shi, D. M., Yang, Y. K., et al. (2019). Antimetastatic effect of fucoidan-sargassum against liver cancer cell invadopodia formation via targeting integrin alphaVbeta3 and mediating alphaVbeta3/Src/E2F1 signaling. *Journal of Cancer, 10*(20), 4777–4792.

Peelen, D., Kodoyianni, V., Lee, J., Zheng, T., Shortreed, M. R., & Smith, L. M. (2006). Specific capture of mammalian cells by cell surface receptor binding to ligand immobilized on gold thin films. *Journal of Proteome Research, 5*(7), 1580–1585.

Qin, N., Lu, S., Chen, N., Chen, C., Xie, Q., Wei, X., et al. (2019). Yulangsan polysaccharide inhibits 4T1 breast cancer cell proliferation and induces apoptosis in vitro and in vivo. *International Journal of Biological Macromolecules, 121*, 971–980.

Ren, R., Gong, J., Zhao, Y., Zhuang, X., Ye, Y., & Lin, W. (2017). Sulfated polysaccharides from *Enteromorpha prolifera* suppress SREBP-2 and HMG-CoA reductase expression and attenuate non-alcoholic fatty liver disease induced by a high-fat diet. *Food & Function, 8*(5), 1899–1904.

Ren, R., Yang, Z., Zhao, A., Huang, Y., Lin, S., Gong, J., et al. (2018). Sulfated polysaccharide from *Enteromorpha prolifera* increases hydrogen sulfide production and attenuates non-alcoholic fatty liver disease in high-fat diet rats. *Food & Function, 9*(8), 4376–4383.

Shao, L. L., Xu, J., Shi, M. J., Wang, X. L., Li, Y. T., Kong, L. M., et al. (2017). Preparation, antioxidant and antimicrobial evaluation of hydroxamated degraded polysaccharides from *Enteromorpha prolifera*. *Food Chemistry, 237*, 481–487.

Shao, W., Zhang, H., Duan, R., Xie, Q., Hong, Z., & Xiao, Z. (2019). A rapid and scalable integrated membrane separation process for purification of polysaccharides from *Enteromorpha prolifera*. *Nature Product Research, 33*(21), 3109–3119.

Shi, M. J., Wei, X., Xu, J., Chen, B. J., Zhao, D. Y., Cui, S., et al. (2017). Carboxymethylated degraded polysaccharides from *Enteromorpha prolifera*: Preparation and in vitro antioxidant activity. *Food Chemistry, 215*, 76–83.

Synytsya, A., Kim, W.-J., Kim, S.-M., Pohl, R., Synytsya, A., Kvasnička, F., et al. (2010). Structure and antitumour activity of fucoidan isolated from sporophyll of Korean brown seaweed *Undaria pinnatifida*. *Carbohydrate Polymers, 81*(1), 41–48.

Tang, Z., Gao, H., Wang, S., Wen, S., & Qin, S. (2013). Hypolipidemic and antioxidant properties of a polysaccharide fraction from *Enteromorpha prolifera*. *International Journal of Biological Macromolecules, 58*, 186–189.

Teng, Z., Qian, L., & Zhou, Y. (2013). Hypolipidemic activity of the polysaccharides from Enteromorpha prolifera. *International Journal of Biological Macromolecules, 62*, 254–256.

Wang, S., Wang, W., Hou, L., Qin, L., He, M., Li, W., et al. (2020). A sulfated glucuronorhamnan from the green seaweed Monostroma nitidum: Characteristics of its structure and antiviral activity. *Carbohydrate Polymers, 227*, 115280.

Wang, Z., Zhang, Z., Zhao, J., Yong, C., & Mao, Y. (2019). Polysaccharides from enteromorpha prolifera ameliorate acute myocardial infarction in vitro and in vivo via up-regulating HIF-1alpha. *International Heart Journal, 60*(4), 964–973.

Wei, J., Wang, S., Liu, G., Pei, D., Liu, Y., Liu, Y., et al. (2014). Polysaccharides from Enteromorpha prolifera enhance the immunity of normal mice. *International Journal of Biological Macromolecules, 64*, 1–5.

Xu, J., Xu, L. L., Zhou, Q. W., Hao, S. X., Zhou, T., & Xie, H. J. (2015). Isolation, purification, and antioxidant activities of degraded polysaccharides from Enteromorpha prolifera. *International Journal of Biological Macromolecules, 81*, 1026–1030.

Ye, H., Shen, Z., Cui, J., Zhu, Y., Li, Y., Chi, Y., et al. (2019). Hypoglycemic activity and mechanism of the sulfated rhamnose polysaccharides chromium(III) complex in type 2 diabetic mice. *Bioorganic Chemistry, 88*, 102942.

Yin, Z., Zhang, W., Zhang, J., Liu, H., Guo, Q., Chen, L., et al. (2019). Two novel polysaccharides in *Psoralea corylifolia* l and anti-A549 lung cancer cells activity in vitro. *Molecules, 24*(20).

Yu, Y., Li, Y., Du, C., Mou, H., & Wang, P. (2017). Compositional and structural characteristics of sulfated polysaccharide from Enteromorpha prolifera. *Carbohydrate Polymers, 165*, 221–228.

Yuan, X., Zheng, J., Ren, L., Jiao, S., Feng, C., Du, Y., et al. (2019). Enteromorpha prolifera oligomers relieve pancreatic injury in streptozotocin (STZ)-induced diabetic mice. *Carbohydrate Polymers, 206*, 403–411.

Zhang, F., Zheng, L., Cheng, S., Peng, Y., Fu, L., Zhang, X., et al. (2019). Comparison of the interactions of different growth factors and glycosaminoglycans. *Molecules, 24*(18).

Zhang, J. J., Zhang, Q. B., Wang, J., Shi, X. L., & Zhang, Z. S. (2009). Analysis of the monosaccharide composition of fucoidan by Precolumn derivation HPLC. *Chinese Journal of Oceanology and Limnology, 27*(3), 1–5.

Zhang, X., Ibrahimi, O. A., Olsen, S. K., Umemori, H., Mohammadi, M., & Ornitz, D. M. (2006). Receptor specificity of the fibroblast growth factor family. *The Journal of Biological Chemistry, 281*(23), 15694–15700.